ELSEVIER

SPECTROCHIMICA ACTA PART B

Spectrochimica Acta Part B 54 (1999) 1351–1365

www.elsevier.nl/locate/sab

Inductively coupled plasma mass spectrometric study of non-linear calibration behavior during laser ablation of binary Cu–Zn Alloys

O.V. Borisov[a], X.L. Mao[a], A. Fernandez[b], M. Caetano[b], R.E. Russo[a,*]

[a] *Lawrence Berkeley National Laboratory, Berkeley, CA 94720, USA*
[b] *Escuela de Quimica, Universidad Central Venezuela, P.O. Box 47102, Caracas 1020-A, Venezuela*

Received 9 April 1999; accepted 7 June 1999

Abstract

Laser ablation behavior of a suite of 10 Cu–Zn binary alloys was studied using inductively coupled plasma mass spectrometry. Three laser systems (20 ns KrF excimer, 6 ns and 35 ps Nd:YAG) were used for ablation. Non-linear calibration plots for both Cu and Zn were observed using all three lasers, despite significant differences in laser ablation mechanisms and good stoichiometry of ablated mass. Crater volume measurements were used to determine the amount of mass removed during repetitive laser ablation from each sample. A change in mass ablation rate for samples with different composition explains observed phenomena. Despite the differences in ablation behavior of these alloys, linear calibration curves were obtained when Zn signal intensity was normalized to signal intensity of Cu or to crater volume.

Keywords: Laser ablation; Inductively coupled plasma; Mass spectrometry; Cu and Zn binary alloys; Brass materials; Calibration

1. Introduction

Development of laser ablation (LA) sampling for chemical analysis is supported by the need to directly characterize various solid samples, including environmental and geological samples, thin films, semiconductors, and others [1–19]. Minimal amount of sample and/or no sample preparation, and reduced amounts of waste are only some of the benefits that make laser ablation a technology of choice compared to conventional liquid nebulization sample introduction, when the original sample is in the solid form. To date, laser abla-

* Corresponding author. Tel.: +1-510-486-4258; fax: +1-510-486-7303.
E-mail address: rerusso@lbl.gov (R.E. Russo)

0584-8547/99/$ - see front matter
PII: S0584-8547(99)00083-X

tion has not experienced the extent of studies as has liquid nebulization; many years of research have been devoted to accurate digestion procedures. What is needed is a commitment to the research to solve the impediments — similar to what has been done for many years with liquid nebulization.

Successful applicability of laser ablation sampling for chemical analysis depends on several criteria. Among these are: sampling a sufficient and known amount of mass; spot-to-spot reproducible sampling; absence of matrix effects, such as different ablation rates, preferential vaporization, or fractionation; and quantitative entrainment and transfer of the ablated mass to the detection system. However, mass ablation rate is a function of the sample composition [20–23] and preferential vaporization of low melting/boiling point elements can occur [24]. To understand these phenomena, numerous studies have addressed laser-ablation sampling using a variety of laser and sample conditions. Encouragingly, UV lasers with short pulse durations provide higher ablation rates, as well as good stoichiometry of the ablated mass [22,24,25]. By understanding mechanisms influencing the mass ablation rate and stoichiometry, laser ablation sampling can evolve into a routine chemical analysis tool.

Laser ablation of brass alloys demonstrates the potential for elemental fractionation; brass seems to represent a worst case scenario [24,26–29]. It has been shown that laser ablation with UV picosecond (ps) pulses and power densities of several Gigawatts per centimeter squared provides Zn/Cu ratios very close to that in the bulk sample. However, the wrong choice of laser power density can provide inaccurate, non-stoichiometric ratios. The low melting/boiling temperatures of Zn are believed to be responsible for Zn-enrichment in the ablated mass; thermal vaporization significantly influences the ablation processes when low power density, long-pulse duration laser are used for ablation [28]. A thermal model of evaporation from a brass surface was successfully used to predict the Zn/Cu inductively coupled plasma atomic emission spectroscopy (ICP-AES) signal intensity ratios for 30-ns KrF excimer laser ablation of brass at low power densities [24]. As power density was increased above 0.3 GW/cm^2, the Zn/Cu ratio did not follow thermal evaporation predictions, but instead became close to the stoichiometric value. As laser pulse duration decreases, non-thermal mechanisms of ablation become significant. In addition, an order of magnitude increase in the amount of ablated mass was measured for a ps-laser ablation compared to a nanosecond (ns) laser, for the same fluence and energy [25]. These studies have demonstrated how the laser–material interaction can be regulated simply by changing the power density.

The dependence of mass ablation rate on matrix forces the use of matched standards for calibration. However, 'good' standards may be unavailable, especially for complex environmental samples. Normalization of analytical data to the acoustic signal generated during laser ablation and to the excitation temperature in the laser-induced plasma (LIP), were successfully used to correct for ablation-rate differences [23]. However, if the extent of elemental fractionation is different for different samples, these normalization techniques fail, and matrix matching is required.

Recently, Gagean and Mermet [29] reported poor Cu calibration for a series of brass samples during LA-ICP-AES experiments. The authors reported an enhancement of Zn signal intensity as Zn concentration in brass increased, resulting in non-linear calibration plots for this element. This enhancement was suppressed, however, when Nd:YAG laser at 266 nm and high power density above 80 GW/cm^2 were used for laser ablation. In their discussion of possible reasons for poor calibration data, the authors stated that sample origin and sample structure, related to thermal treatment during sample preparation, may have influenced the observed behavior.

LA-ICP mass spectrometry (MS) of binary Cu–Zn alloys was investigated in this work to further address the non-linear calibration issue. Significant differences in physical properties, such as melting and boiling temperatures of Cu and Zn make these binary alloys 'difficult' samples for

laser ablation. The approach in this work was to first establish laser ablation conditions where the Zn/Cu ratio of the ablated mass was close to stoichiometric. Secondly, we studied whether elemental fractionation was the same or different for alloys with different Zn/Cu ratio in the bulk. Thirdly, as reported by Gagean and Mermet [29], we sought to determine if the non-linear calibration behavior for Cu and Zn was attributed to different thermal treatment and different origin of the samples. Thus, the basis of this work is to study how different laser ablation conditions affect Zn and Cu calibration behavior. In this case, three laser systems: a ns excimer, and a ns and ps Nd:YAG laser were used for ablation of the brass alloys. The binary Cu–Zn alloys were of the same origin with similar thermal treatment to exclude possible origin-related differences in the samples. Crater volumes, after repetitive ablation of a sample, were measured with a white-light interferometric microscope, and these data were used to relate the amount of ablated mass with ICP-MS signal intensities.

2. Experimental

The experimental system includes three laser systems, a PQ3 (VG Elemental) inductively coupled plasma mass spectrometer (ICP-MS) equipped with simultaneous mode detector, and an ablation cell. The lasers include: a Nd:YAG (New Wave Research) frequency quadrupled (266 nm) with a 6-ns pulse width, a KrF excimer (Lambda Physik) with a 30-ns pulse width at 248 nm, and a Nd:YAG (Continuum) frequency doubled (532 nm) with a 35-ps pulse width. Instrumentation and experimental conditions used in this work are summarized in Table 1. The laser beam was attenuated prior to focusing and transferred to a sample surface by means of series of mirrors. A plano-convex lens with a nominal focal length of 20-cm was used in the ablation experiments with the KrF and the ns and ps Nd:YAG lasers. All lasers were operated at 10 Hz repetition rate. The laser beam energy from the ns Nd:YAG laser was adjusted with a built-in optical attenuator. Due to the fact that this beam was only 2 mm in diameter, an optical beam expander was used before the lens to achieve better focusing of the beam onto the sample surface. The KrF excimer laser beam energy was attenuated with a series of beam splitters placed in the beam path to give a final energy for ablation of approximately 1.0 mJ/pulse. The beam energy from the ps Nd:YAG was adjusted using a variable wedge attenuator (Model 935-10, Newport Corporation).

The laser beam spot diameter was measured by using a single laser pulse with low energy (approx. 200 μJ) to cause melting on a single crystal Si sample. Ablation craters were measured using a white-light interferometric microscope (New View

Table 1
Instrumentation and laser-ablation experimental conditions

Laser systems	KrF excimer	Nd:YAG	Nd:YAG
Pulse duration	30 ns	6 ns	35 ps
Energy (mJ)	1.25	1.10	1.00
Power density (GW/cm^2)	1.71	2.30	168.0
Repetition rate (Hz)	10	10	10
Wavelength (nm)	248	266	532
Detection system	Quadrupole ICP-MS (PQ3,VG elemental)		
Power (W)	1350		
Plasma Ar gas flow rate (l/min)	14		
Auxiliary Ar gas flow rate (l/min)	0.8		
Carrier Ar gas flow rate (l/min)	0.9		
ICP-MS dwell time (ms)	24		
Intensity integration time (s)	6		
Analytes	Cu^{63} 69.09% abundant, Zn^{64} 48.6% abundant		

200, Zygo Corporation). The software, supplied with this microscope allows crater parameters such as depth, width, and volume to be determined. Crater volume, above and below a reference surface, can be determined. In this work, net ablated crater volume is defined as the volume below a reference surface minus the volume above this surface. The sample surface, not ablated by laser irradiation, was used as the reference. Considerable effort was made to achieve a uniform laser beam profile and craters, which could be reliably measured. If laser power density was too high and spot size too small, crater aspect ratio and a very sharp rim surrounding a crater, did not allow for the reliable volume data to be measured.

A description of the ablation chamber can be found elsewhere [30]. Samples were placed on an XYZ translation stage with manual controls. ICP-MS signal intensity data were acquired in the time-resolved mode during continuous ablation on a single sample surface, using time-resolved analysis (TRA) software supplied with the instrument. Due to the transient nature of the signal from laser ablation, a short dwell time of 24 ms/peak and single peak per isotope were used throughout these experiments. In most cases, data reduction was performed by averaging signal intensities over 6-s time intervals, unless otherwise specified. The reported data represent an average

Table 2
Cu–Zn binary alloys composition (Glen Spectra Reference Materials)

Samples: Cu–Zn binary alloys	Cu wt.%	Zn wt.%
Sample #1	51.48	48.52
Sample #2	55.6	44.4
Sample #3	60.6	39.3
Sample #4	65.2	34.7
Sample #5	69.5	30.5
Sample #6	74.8	25.2
Sample #7	82.0	18.0
Sample #8	85.1	14.9
Sample #9	89.5	10.5
Sample #10	93.8	6.2

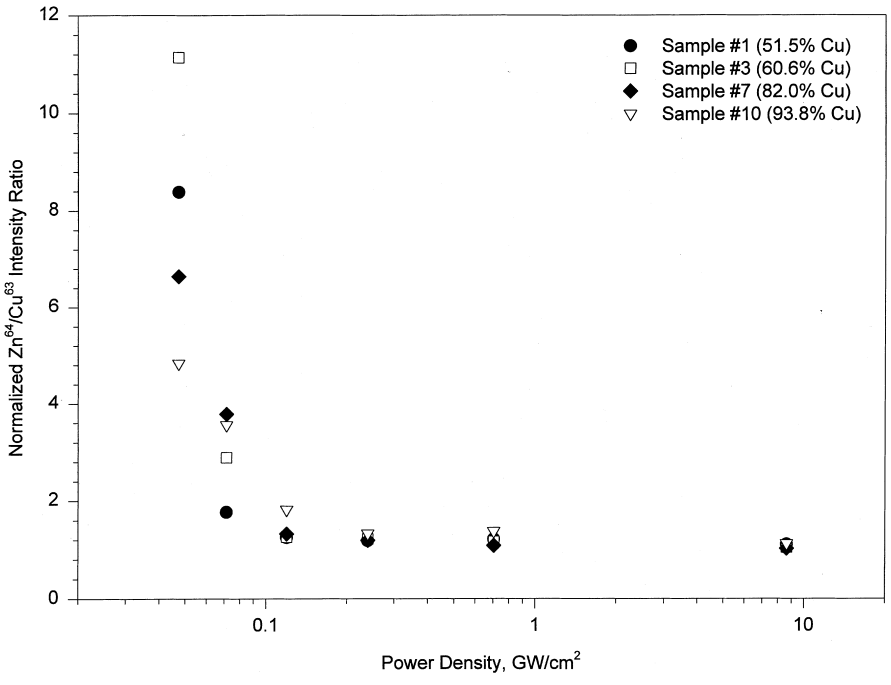

Fig. 1. Zn^{64}/Cu^{63} signal intensity ratio after 120 s of pre-ablation, normalized to certified bulk ratio, as a function of KrF excimer laser power density.

of laser ablation on three, randomly selected areas on the sample surface. ICP-MS operating parameters were optimized to provide a sufficient number of counts without saturating the detector (operated in a pulse counting mode), achieved by changing the voltages applied to the ion-optic elements. This procedure was necessary because isotopes of the major elements in the samples were analyzed.

Samples used in this study were a suite of 10 binary copper–zinc alloys (Glen Spectra Reference Materials, England) of various composition. Zn concentration in these samples ranged from 6.2 to 48.5 wt.% (see Table 2 for details). The samples were polished and kept in an evacuated dessicator.

3. Results and discussion

3.1. Thirty nanosecond KrF excimer laser ablation

Fractionation during laser ablation of brass is a well-known phenomenon. In fact brass probably represents a worst case for analytical purposes, but an ideal case for studying laser ablation

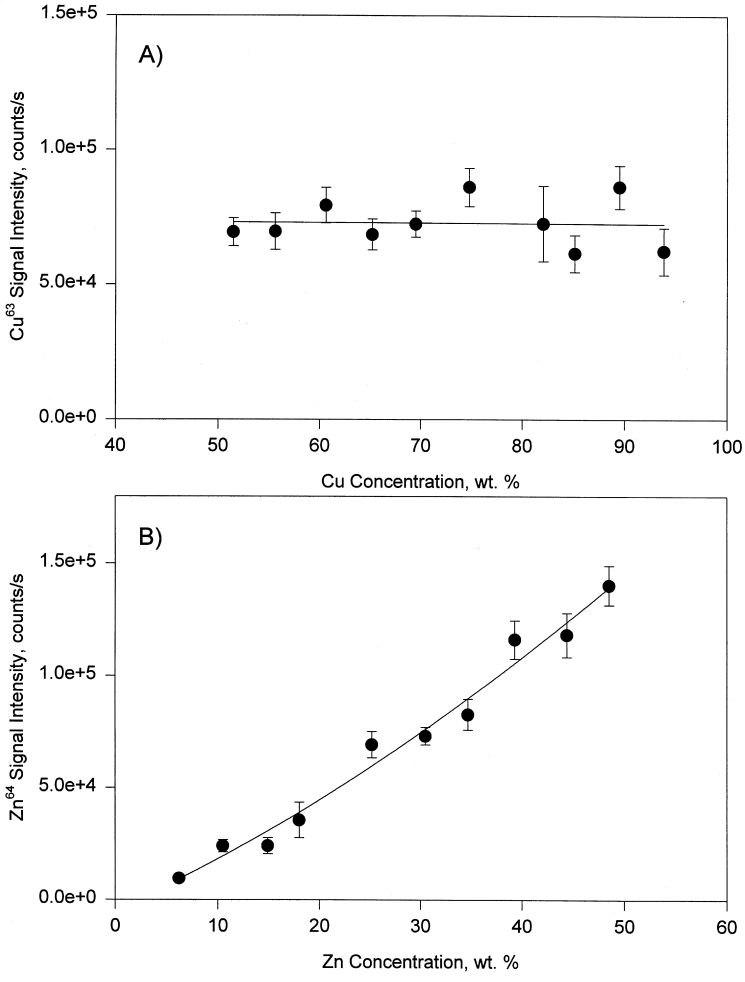

Fig. 2. Calibration curves for Cu (A) and Zn (B) with 120 s of pre-ablation as a result of ablation of binary Cu–Zn alloys with KrF excimer laser.

mechanisms because the degree of fractionation significantly depends on the laser power density. The data in Fig. 1 show the dependence of Zn^{64}/Cu^{63} ICP-MS signal intensity ratio on laser power density for several copper–zinc binary alloys during KrF excimer laser ablation. The data are normalized to the certified ratio in each of the samples. At low power density, the measured ratios are significantly larger than the stoichiometric values, indicating a high degree of fractionation at these power densities. The degree of fractionation for samples with different compositions also can be different, however, no clear trend was seen for these samples at low power densities. As power density increases to greater than ~ 0.2 GW/cm^2, the ratio decreases and reaches certified values, indicating no significant fractionation at the higher laser power densities. This power density region would be ideal for chemical analysis. To minimize and/or eliminate fractionation and study calibration behavior in this work, a KrF excimer laser power density larger than 0.2 GW/cm^2 was used.

Copper and Zn calibration plots, obtained during laser ablation of these binary alloys at power density of 1.7 GW/cm^2 are shown in Fig. 2. ICP-MS Cu signal intensity is almost independent of Cu concentration in these samples, whereas Zn signal intensity non-linearly increases with Zn concentration. Similar behavior of calibration graphs was recently reported by Gagean and Mermet [29]. The measured non-linearity of calibration plots for Cu and Zn in these alloys is an interesting phenomenon from a fundamental point of view.

ICP-MS ion counts from both Cu and Zn isotopes, measured during ablation of these binary alloys, is defined here as the total ion count, and is assumed to be proportional to the amount of ablated mass/unit time (ablation rate). The validity of this assumption depends on the transport efficiency of the ablated mass. Transport efficiency is determined by the particle size distribution. It is assumed that particle size distribution does not significantly change for the suite of Cu–Zn binary alloys. The total ion count, as a

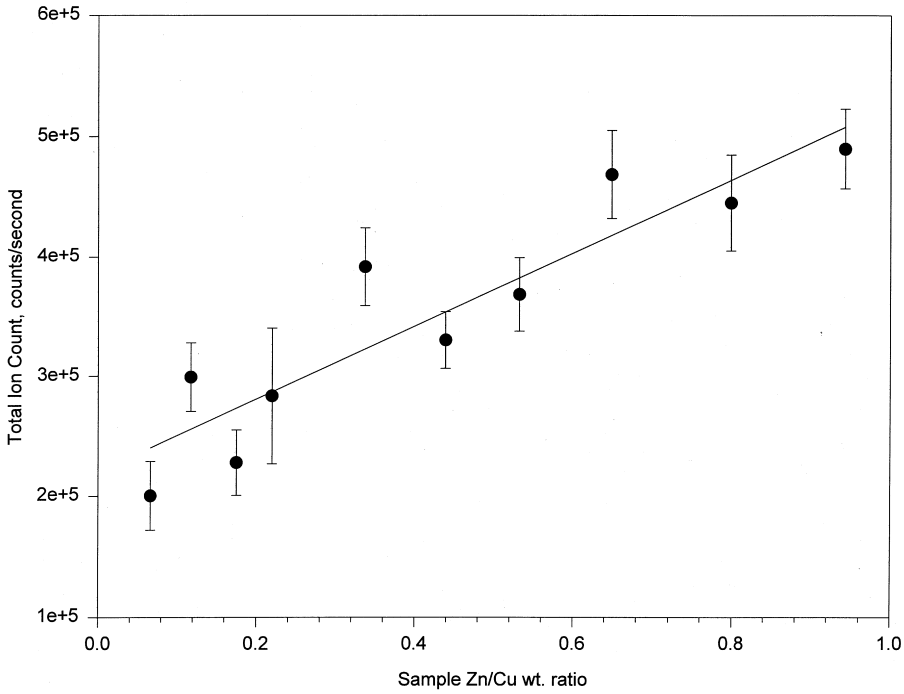

Fig. 3. ICP-MS total ion counts as a function of Zn/Cu ratio in the sample after 120 s of pre-ablation with KrF excimer laser.

function of Zn/Cu ratio in each sample, is shown in Fig. 3. The total ion count increases with increasing Zn concentration in the binary alloys for the same laser power density. Assuming transport efficiency is similar, the ablation rate is different for the suite of binary Cu–Zn alloys, increasing with increasing Zn concentration. From these data, it follows that the amount of ablated mass must be a function of sample composition, possibly explaining the Zn and Cu calibration non-linearities.

Reference to an internal standard is frequently used in chemical analysis to correct for differences in laser ablation sampling efficiency and instrument response. Different ablation rates, observed in the suite of alloys can be compensated for by normalization of experimental data to the signal intensity of a matrix element. When Cu was used as an internal standard, a linear calibration curve (ICP-MS Zn^{64}/Cu^{63} intensity ratio vs. certified Zn/Cu ratio in the sample) for Zn with correlation coefficient, R^2, of 0.998 and slope of 1.10 ± 0.01 was measured. These data demonstrate how internal standardization successfully corrects for different ablation rates in the series of binary Cu–Zn alloys.

3.2. Thirty-five picosecond Nd:YAG laser ablation

Laser ablation using ps pulses provides enhanced sensitivity and improved accuracy [24]. Power density dependence of Zn/Cu ratios measured during ps-laser ablation is significantly different from ablation with the 30-ns excimer laser pulses. ICP-MS Zn/Cu ratios, normalized to the certified bulk levels, during ablation with ps-laser are shown in Fig. 4 for three alloys. The Zn/Cu ratios increase slightly as laser power density increases, but the ratios for different samples follow each other more closely than in the ns-laser case (cf. Fig. 1). At power densities above 10 GW/cm^2, the ratio composition is stoichiometric.

Providing that ps-pulsed laser ablation mechanisms are different than those from longer ns-pulses, one may expect that calibration curves for the suite of binary Cu/Zn alloys may be differ-

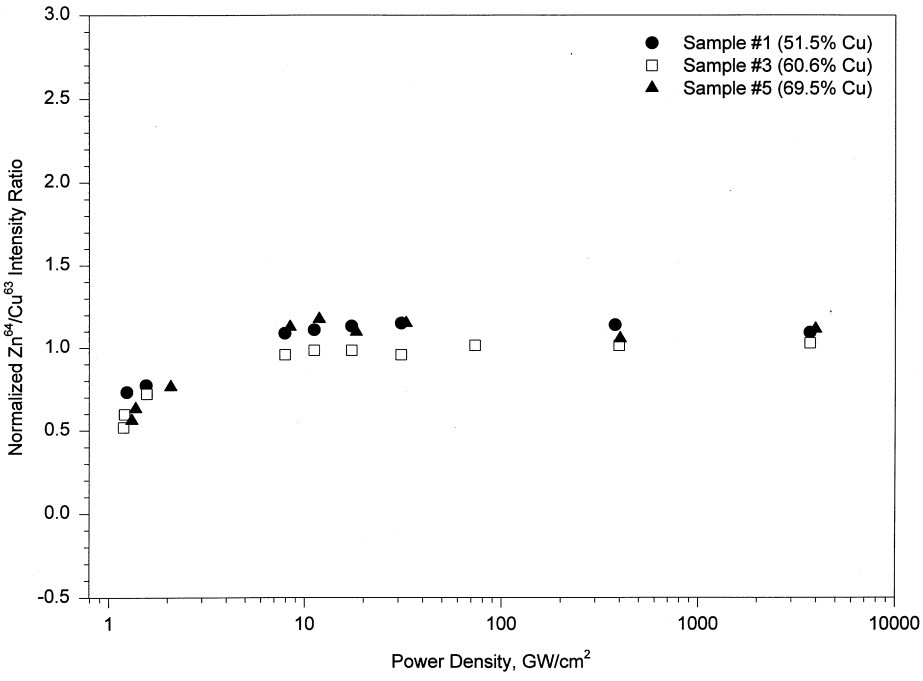

Fig. 4. Zn^{64}/Cu^{63} signal intensity ratio after 60 s of pre-ablation, normalized to the certified ratio in the bulk, as a function of power density during ps-Nd:YAG laser ablation with 532-nm pulses.

ent. However, when the signal intensities for Cu and Zn were plotted against their concentration in the sample, non-linear calibrations also were observed, as shown in Fig. 5. The calibration curve for Cu had a negative slope; signal intensity decreased as Cu concentration in the sample increased. On the other hand, Zn signal intensity was significantly enhanced as Zn concentration in the sample increased. The non-linear calibration behavior is very similar to that shown for 30-ns-pulsed excimer laser ablation (cf. Fig. 2) despite significant differences in laser ablation conditions and mechanisms.

As in the case of ns-pulsed excimer laser ablation, a good calibration curve can be obtained by rationing the Zn signal intensity to that of Cu. A calibration, presented as Zn^{64}/Cu^{63} intensity ratio as a function of Zn/Cu concentration ratio, with slope of 0.998 ± 0.01 and correlation coefficient, R^2, of 0.996 was achieved.

3.3. Six nanosecond Nd:YAG laser ablation and crater measurements

The non-linear behavior of Cu and Zn in these binary alloys was investigated further using a 6-ns

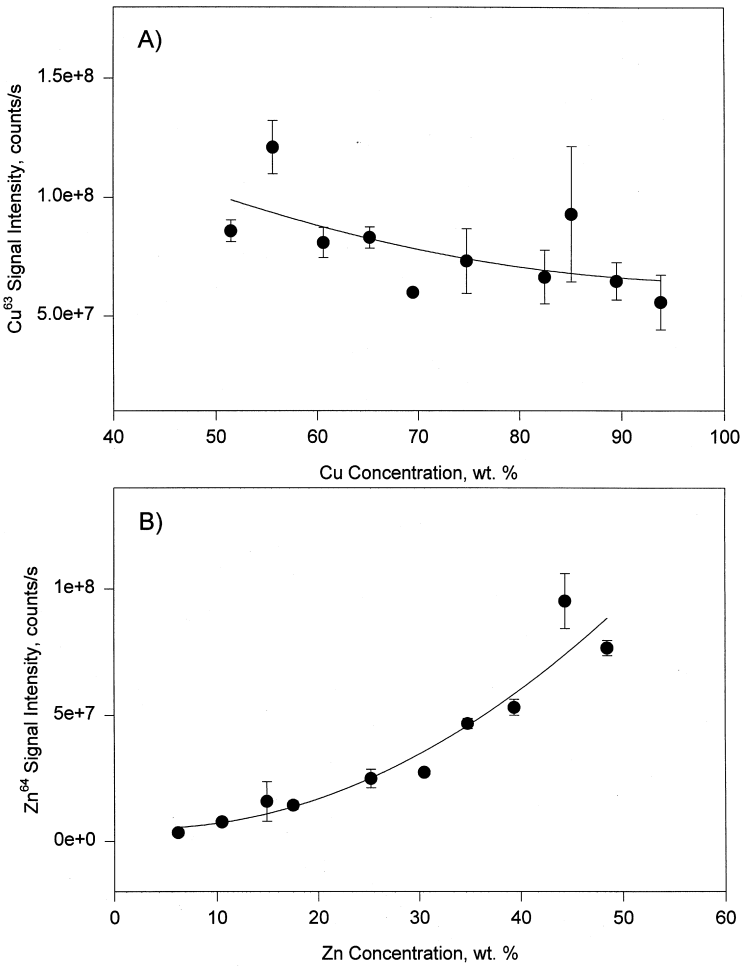

Fig. 5. Calibration curves after 60 s of pre-ablation for Cu (A) and Zn (B) as a result of ablation of binary Cu–Zn alloys with ps-Nd:YAG laser.

Table 3
Calibration plots (Zn^{64}/Cu^{63} vs. Zn/Cu concentration ratio) for analysis of Cu–Zn binary alloys after different ablation times[a]

Ablation time (s)	Slope	Correlation coefficient R^2
10	0.553 ± 0.007	0.996
30	0.526 ± 0.006	0.998
45	0.543 ± 0.005	0.999

[a]Cu is used as an internal standard. Laser energy and power density are, respectively, 1.10 mJ and 2.3 GW/cm^2.

pulsed Nd:YAG laser. In this case, the spatial profile of the laser beam was expanded and apertured so that its spatial profile was essentially a top-hat power distribution. The improved beam quality of this laser insures that the energy density is constant across the diameter of the spot, which facilitates measurement of the craters in the samples (cleaner crater). A strong time dependence of Cu and Zn signals, for both ICP-AES and MS detection, during continuous laser ablation is well documented [26,31]. Thus, it is

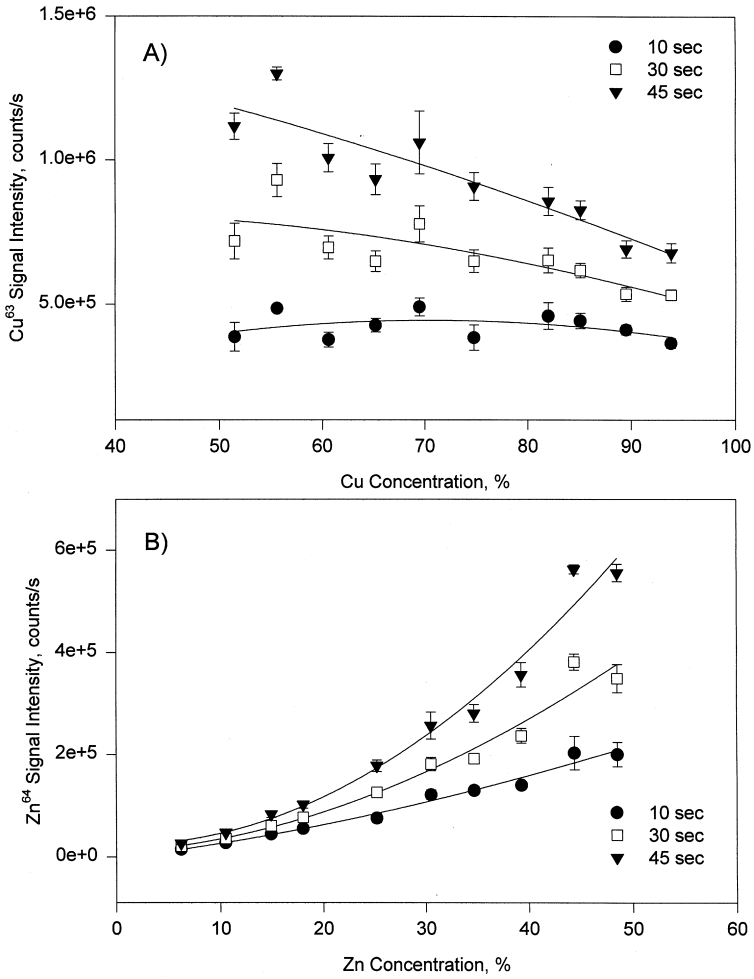

Fig. 6. Calibration curves for Cu (A) and Zn (B) as a result of ablation of binary Cu–Zn alloys. Five second integration time after 10 (●), 30 (□), and 45 (▼) s of ablation with ns-Nd:YAG laser.

important to investigate the effect of this time dependence on analytical calibration and ensure that the non-linear behavior is not a manifestation of time. Cu and Zn calibration curves are plotted for 5-s integration intervals at the different times of 10, 30, and 45 s after the start of ablation (Fig. 6). As seen from the data in Fig. 6, Cu signal intensity does not increase with Cu concentration in the samples in contrast to the non-linear increase of the Zn signal, as its concentration in the series increases. At 10 s of ablation, the Cu signal is almost independent of Cu content in the sample. As ablation time increases, Cu calibration graphs gain a negative slope, especially seen by examining the Cu behavior after 45 s of ablation. At the same times the shape of the Zn calibration plots becomes more non-linear with an increasing value for a second order coefficient using polynomial curve fitting equation. This behavior cannot be attributed to changes in degree of fractionation at different ablation times; Zn^{64}/Cu^{63} ratios did not change with time for each of the alloys at this laser power density. However, for each case (time) when Zn signal intensity was rationed to that of Cu, linear calibration curves were established; Table 3 summarizes these results. It is clearly seen that Cu can be used as an internal standard for Zn analyses in these Cu–Zn samples despite the non-linear behavior of the individual species. Thus, by rationing the Zn signal intensity to that of Cu, correction for different ablation behavior in these difficult alloys is achieved.

One way to investigate the behavior of the Cu and Zn in these alloys is to measure the volume of the craters formed after laser ablation. A typical depth profile across a crater, formed after 45 s of repetitive ablation at power density of 2.3 GW/cm^2, is shown in Fig. 7. Craters are characterized by a relatively flat bottom with evidence of melting and a sharp rim. The laser power density of 2.3 GW/cm^2 was used to ensure measurable craters and to provide stoichiometric ablation. If power density is increased by decreasing the spot size, deep narrow craters with a sharp tall rim makes volume measurements difficult, especially for longer sampling times.

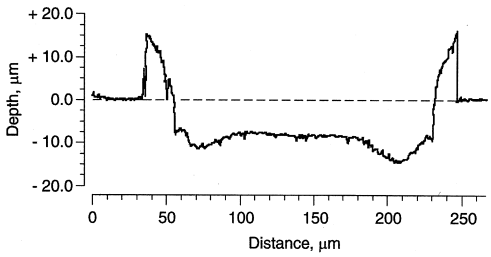

Fig. 7. Cross-section profile of a crater, formed after 45 s of repetitive ns-Nd:YAG laser ablation of Cu–Zn alloy sample, measured with a white-light interferometric microscope.

Laser ablation craters were measured for all the binary Cu–Zn alloys used in this work. A good correlation was established between the total ICP-MS ion count for both Cu and Zn isotopes and the net crater volume data (Fig. 8). Due to the transient nature of laser ablation, total counts were calculated as an integrated signal intensity for both Cu and Zn isotopes over 45 s of laser ablation, minus background (signal recorded with no laser ablation). The volume measurements represent the average of three craters in each of the 10 different samples. These data demonstrate how the signal intensity is influenced by sample-specific changes in the amount of ablated mass, i.e. the ablation rate. The amount of ablated mass is different for different samples, increasing with increasing Zn concentration in the samples.

The mass ablation rate was examined for samples with high and low Zn concentration (sample nos. 2 and 10) in more detail. Laser ablation craters, after laser ablation with 1, 5, 10, 50, 200, and 500 laser pulses, were used to determine the mass ablation rate. Densities of 8.4 and 8.8 g/cm^3 were used in converting volume data to mass, respectively, for samples nos. 2 and 10. Results are summarized in Table 4. The mass ablation rate depends on sample composition, and is approximately 3.5 times less for samples with lower Zn contents. Addition of Zn to the Cu matrix improves the mass ablation rate. Formation of a rim, defined as the mass above the sample surface, is essentially the same for the two samples. Properties of the molten layer such as

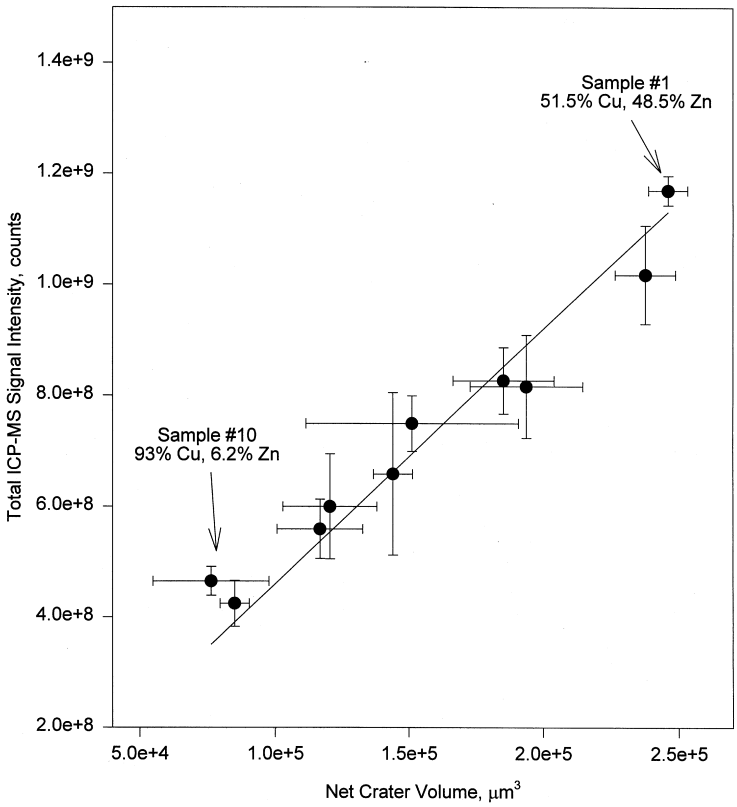

Fig. 8. Correlation between total ion counts and a net crater volume after repetitive ns-Nd:YAG laser ablation of the suite of Cu–Zn binary alloys. Data corresponding to samples nos. 1 and 10 are indicated on the graph.

depth, surface tension, and area of the molten pool determine crater shape and thus the amount of mass re-solidified into a rim.

Measurements of crater volume clearly demonstrate that the amount of ablated mass is a strong function of the Cu–Zn alloy composition. This mass-ablation rate dependence causes the non-linearity of calibration curves for Cu and Zn as shown in Fig. 6. A decrease in the amount of ablated mass with increasing Cu concentration in the samples results in a zero or even negative slope for Cu calibration curves, depending on the ablation time. In contrast, Zn signal from samples with larger Zn concentration is enhanced due, to increased amounts of mass entering the ICP. As shown in Fig. 9(A), the net crater volume linearly correlates with the Zn/Cu ratio in the samples. Based on this behavior, one can estimate the approximate shape of calibration curves for Zn and Cu as a result of laser ablation of these alloys. Defining M as a total ablated mass, the correlation between ablated mass and Zn-to-Cu certified concentration ratio, R, is given by:

Table 4
Coefficient γ (ng/pulse), mass ablation rate, for equation: *Mass* $= \gamma$ * *Pulse Number*, during ns-Nd:YAG laser ablation of two Cu–Zn binary alloys[a]

Mass (ng)	Sample #2: 55.6% Cu, 44.4% Zn	Sample #10: 93.8% Cu, 6.2% Zn
Above the surface	1.27 ± 0.05	1.52 ± 0.03
Below the surface	6.2 ± 0.1	2.9 ± 0.1
Net ablated mass	5.0 ± 0.2	1.4 ± 0.1

[a] Laser power density is 2.3 GW/cm^2.

$$M = \alpha + \beta \times R \quad (1)$$

with α and β coefficients determined from experimental data to be 0.67 ± 0.05 μg and 1.6 ± 0.1 μg, respectively. During laser ablation of these binary Cu–Zn alloys, the total mass M is equal to $m_{Zn} + m_{Cu}$, where m_{Zn} and m_{Cu} are, respectively, the mass of ablated Zn and Cu. Providing that the ablation is stoichiometric (which is accurate at the power density used here), the ratio m_{Zn}/m_{Cu} is proportional to the Zn/Cu concentration ratio in a sample. Because the signal intensity for Cu and Zn is proportional to ablated mass, one can show that:

$$I_{Cu} = B \times m_{Cu} = B \times \frac{\alpha + \beta \times R}{R + 1} \quad (2)$$

$$I_{Zn} = A \times m_{Zn} = A \times \frac{(\alpha + \beta \times R) \times R}{R + 1} \quad (3)$$

$$\frac{I_{Zn}}{I_{Cu}} = \frac{A}{B} \times R \quad (4)$$

where I_{Zn} and I_{Cu} are the ICP-MS signal intensities from Zn and Cu isotopes, A and B are correlation coefficients, and R is the certified Zn/Cu ratio. Coefficients A and B incorporate

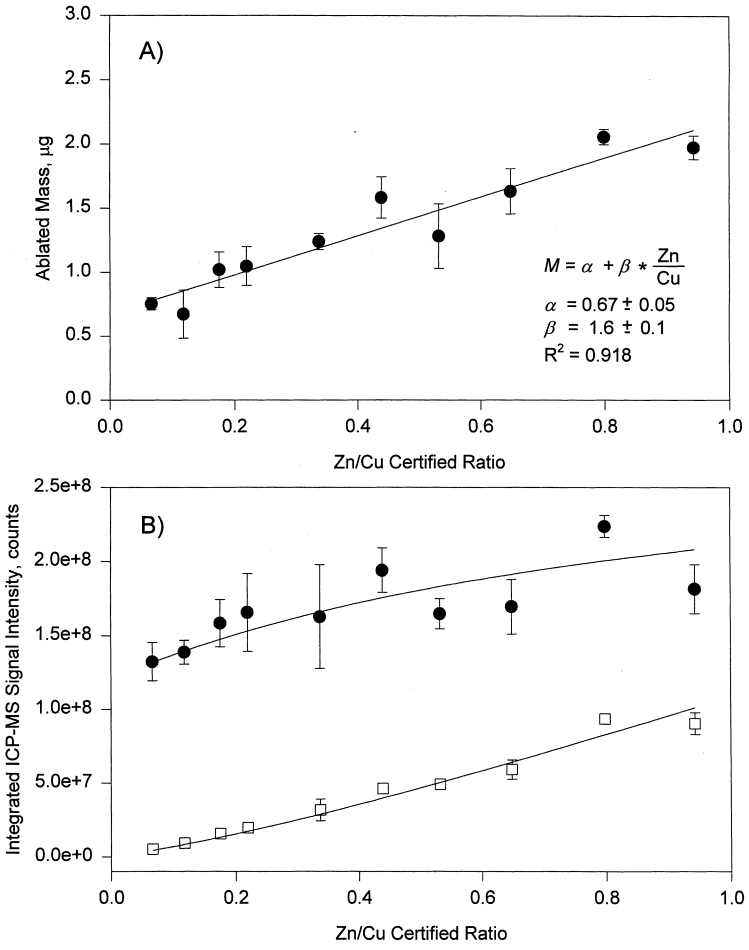

Fig. 9. Amount of laser ablated mass (μg) (A) and integrated signal intensity for Cu^{63} (●) and Zn^{64} (□) (B) as a function of Zn/Cu certified ratio in a sample. Solid lines in B are results of fitting experimental data with Eqs. (2) and (3), respectively, for Cu and Zn. Total ablation time was 45 s.

instrument sensitivity, mass transport from the ablation site to the torch, differences in ionization efficiencies of Zn and Cu in the ICP-MS, and abundances of corresponding isotopes.

Total signal intensities, integrated over 45 s of ablation, for Cu^{63} and Zn^{64} are shown in Fig. 9(B) as a function of Zn/Cu certified level in the samples. Mass ablation dependence on sample composition can be demonstrated by fitting experimental data with Eqs. (2) and (3), using coefficients A and B as the variables and values for α and β, determined from the linear fit with Eq. (1). Results of fitting these experimental data are shown in Fig. 9(B) as solid lines. Coefficients A and B are equal to $(18.3 \pm 0.6) \times 10^7$ counts/μg and $(9.5 \pm 0.3) \times 10^7$ counts/μg, respectively. These data clearly indicate that difficulties in establishing good calibration plots for Cu and Zn during ablation of binary alloys are solely due, to a sample-dependent mass ablation rate even during stoichiometric ablation. Linear dependence of mass ablation rate on Zn-to-Cu ratio in these samples can be compensated for by signal normalization procedures, utilizing Cu as an internal standard. From Eq. (3), it follows that the ratio of Zn signal intensity to that of Cu is independent of the amount of ablated mass and is determined by the ratio of coefficients A and B. The A/B ratio, based on fitting with Eqs. (2) and (3), equals an 0.52 ± 0.03. When experimental data for Zn/Cu signal intensity ratio was plotted as a function of Zn/Cu certified concentration ratio in these samples, linear correlation ($R^2 = 0.998$) was established with a slope of 0.537 ± 0.005. Both values, one directly determined from a slope and the other indirectly derived from A/B ratio, are in excellent agreement.

Successful application of an internal standardization method to chemical analysis of multi-component samples requires knowledge of the internal standard concentration in the standards and in the samples. Unfortunately, this information is not always available, especially for unknown samples. On the other hand, differences in mass ablation rate can be compensated for by normalization of experimental intensity data to total mass removed from a sample surface during repetitive laser ablation. Here, total ablated mass was determined from crater volume measurements. When ablated mass was used for signal intensity normalization, linear calibration plots, defined as

$$\frac{I}{M} = \delta \times C \tag{5}$$

were established. I is integrated Cu^{63} or Zn^{64} signal intensity (counts), M is amount of ablated mass (μg), and C is Cu or Zn concentration (wt.%). Slopes, δ, of $(1.89 \pm 0.03) \times 10^6$ and $(1.02 \pm 0.02) \times 10^6$, and linear correlation coefficients, R^2, of 0.901 and 0.997 were observed, respectively, for Cu and Zn calibration. These data clearly demonstrate that despite different mass ablation rates, characteristic of these binary alloys, linear Cu and Zn calibrations can be established if one knows the amount of ablated mass. From these data and linear calibration plots for Cu and Zn, based on Eq. (5), it seems that particle size distribution does not significantly change for the suite of binary Cu–Zn alloys. Poorer calibration-curve linearity for Cu than for Zn probably comes from narrow dynamic range in Cu concentrations.

The reasons for this mass-ablation-rate behavior are not well established; several factors are likely to play a role. Laser-energy losses due, to heat diffusion into a bulk, energy converted into acoustical waves, energy carried away by a vapor, absorbed, scattered, and reflected by a sample surface and laser-induced plasma energy can all effect the mass ablation rate. The thermal conductivity, which determines heat dissipation into the bulk, for these binary alloys is a non-linear function of sample composition [32]. These changes in thermal conductivity are, thus, unlikely to explain the observed ablation-rate differences for these Cu–Zn alloys. As Zn concentration in the samples increases, melting temperature almost linearly decreases. Melting temperature difference for the alloys with the lowest and the highest Zn concentration is approximately 200°C, changing from approximately 1050°C for the sample with the lowest Zn concentration to approximately 850°C for the sample with the highest Zn concentration. Assuming that the same amount of

laser energy is coupled to each sample, the depth of the molten pool will be effected by the thermal characteristics of a sample. Assuming that ejection of molten particles is a significant contribution to the laser ablation mechanism, more mass will be removed from the sample with the lower melting temperature. However, the different reflectivity of these samples probably plays a significant role in determining the amount of laser energy coupled to each sample surface. To the best of our knowledge, reflectivity data for this suite of binary Cu–Zn alloys is not available, although, reflectivity is expected to change during the laser pulse, further complicating the energy absorption behavior.

4. Conclusion

Non-linearity in calibration graphs during laser ablation of binary Cu–Zn alloys was found to be due to a change in the mass ablation rate, which was related to the relative concentration of Zn and Cu in these alloy samples. An increase of Zn concentration in the bulk samples resulted in an increase in the amount of ablated mass, thus the addition of Zn to brass matrix improves mass ablation rate, probably due to lowering melting temperature of the alloy. Determination of mass ablation rates was done by measuring ablation crater volumes with a white-light interferometric microscope. The amount of ablated mass was a linear function of the certified Zn/Cu ratio in the suite of binary alloys. This dependence explains Zn and Cu calibration-curve non-linearity, reported here and by other researchers. The results were independent of laser pulse width, and were shown to be similar for 30 ns, 6 ns, and 35 ps laser pulses.

Good calibration for the analysis of Cu–Zn binary alloys was possible when signal normalization procedures were used. Two normalization procedures were used in this work, one with Cu as an internal standard and another, external standardization with the amount of ablated mass as an indicator of ablation efficiency. When Zn signal intensity was normalized to that of Cu, linear calibration curves were observed; here, Cu signal intensity corrects for changes in an amount of ablated mass. Different mass ablation rates, characteristic to these alloys, can also be compensated for if one knows an amount of mass ablated and transported to the ICP torch. In this work, amount of ablated mass was determined from crater volume measurements. When integrated signal intensity for Cu^{63} and Zn^{64} was normalized by an amount of ablated mass, linear calibration curves were observed. These results indicate that both normalization procedures can be successfully used in analysis of these samples. Although the understanding of brass ablation has been improved, from a practical viewpoint, routine analysis may still be a problem if knowledge of the internal standard concentration is not available or if external standardization procedures are not available.

Good stoichiometry of ablated mass was achieved during ablation of all 10 binary Cu–Zn alloys at high power densities, despite the differences in ablation mechanism, characteristic to each of the laser systems used in this work. Although Zn and Cu ICP-MS signal intensities exhibit strong time dependence during continuous laser ablation at these high power densities, Zn-to-Cu ratios do not change with time and remained constant. For future work, it will be interesting to study craters at different laser ablation conditions (such as power density and pulse duration), to determine if conclusions made in this work about the sample-dependent mass ablation rate hold true at various laser ablation conditions.

Acknowledgements

This work was supported by the Environmental Management Science Program, funded jointly by the Assistant Secretary for Environmental Management and by the Director, Office of Energy Research, of the US Department of Energy, under Contract No. DE-AC03-76SF00098. A.F. and M.C. thank the Applied Science Division of Lawrence Berkeley Laboratory and University Central of Venezuela (grant C.D.C.H. no. 03-12-4104-98).

References

[1] M.D. Norman, N.J. Pearson, A. Sharma, W.L. Griffin, Geostand. Newslett. 20 (1996) 247.
[2] M. Hemmerlin, J.M. Mermet, M. Berucci, P. Zydowics, Spectrochim. Acta Part B 52 (1997) 421.
[3] S. Kozuka, M. Hayashi, H. Matsunaga, Anal. Sci. 9 (1993) 735.
[4] T. Mochizuki, A. Sakashita, H. Iwata, Y. Ishibashi, N. Gunji, Anal. Sci. 7 (1991) 763.
[5] S.A. Darke, S.E. Long, C.J. Pickford, J.F. Tyson, Fresenius J. Anal. Chem. 337 (1990) 284.
[6] V.V. Kogan, M.W. Hinds, Spectrochim. Acta Part B 49 (1994) 333.
[7] D.S. Zamzow, D.P. Baldwin, S.J. Weeks, S.J. Bajic, A.P. D'Silva, Environ. Sci. Technol. 28 (1994) 352.
[8] S.A. Baker, M. Bi, R.Q. Aucelio, B.W. Smith, J.D. Winefordner, J. Anal. At. Spectrom. 14 (1999) 19.
[9] P.J. Sylvester, M. Ghaderi, Chem. Geol. 141 (1997) 49.
[10] S.E. Jackson, H.P. Longerich, G.R. Dunning, B.J. Fryer, Can. Mineral. 30 (1992) 1049.
[11] B.J. Fryer, S.E. Jackson, H.P. Longerich, Chem. Geol. 109 (1993) 1.
[12] R.J. Watling, H.K. Herbert, I.D. Abell, Chem. Geol. 124 (1995) 67.
[13] W.T. Perkins, N.J.G. Pearce, T.E. Jeffries, Geochim. Cosmochim. Acta 57 (1993) 475.
[14] A. Moissette, T.J. Shepherd, S.R. Chenery, J. Anal. At. Spectrom. 11 (1996) 177.
[15] M. Ducreux-Zappa, J.-M. Mermet, Spectrochim. Acta Part B 51 (1995) 321.
[16] F.E. Lichte, Anal. Chem. 67 (1995) 2479.
[17] D. Günter, R. Frischknecht, C.A. Heinrich, H.-J. Kahlert, J. Anal. At. Spectrom. 12 (1997) 939.
[18] S. Chenery, J.M. Cook, M. Styles, E.M. Cameron, Chem. Geol. 124 (1995) 55.
[19] M.L. Alexander, M.R. Smith, J.S. Hartman, A. Mendoza, D.W. Koppenaal, Appl. Surf. Sci. 127–129 (1998) 255.
[20] R.E. Russo, X.L. Mao, Chemical analysis by laser ablation, Experimental Methods in the Physical Sciences, 30, Academic Press, New York, 1998, pp. 375–412.
[21] M. Gagean, J.M. Mermet, J. Anal. At. Spectrom. 12 (1997) 189.
[22] C. Geertsen, A. Briand, F. Chartier, J.L. Lacour, P. Mauchien, S. Sjöström, J.M. Mermet, J. Anal. At. Spectrom. 9 (1994) 17.
[23] C. Chaléard, P. Mauchien, N. Andre, J. Uebbing, J.L. Lacour, C. Geertsen, J. Anal. At. Spectrom. 12 (1997) 183.
[24] X.L. Mao, A.C. Ciocan, R.E. Russo, Appl. Spectrosc. 52 (1998) 913.
[25] X.L. Mao, O.V. Borisov, R.E. Russo, Spectrochim. Acta. part B 53 (1998) 731.
[26] E.F. Cromwell, P. Arrowsmith, Appl. Spectrosc. 49 (1995) 1652.
[27] J.M. Baldwin, J. Appl. Phys. 44 (1973) 3362.
[28] J.M. Baldwin, Appl. Spectrosc. 24 (1970) 429.
[29] M. Gagean, J.M. Mermet, Spectrochim. Acta, Part B 53 (1998) 581.
[30] A.P.K. Leung, W.T. Chan, X.L. Mao, R.E. Russo, Anal. Chem. 70 (1998) 4709.
[31] O.V. Borisov, X.L. Mao, A.C. Ciocan, R.E. Russo, Appl. Surf. Sci. 127–129 (1998) 315.
[32] S. Aoyama, T. Itô, Nippon Kinzoku Gakkai-shi, J. Jpn. Inst. Met. 4 (1940) 37.